Analyst

Facile and Scalable Fabrication of Molecularly Imprinted Polymer (MIP) Sensors on Poriferous Laser-Engraved Graphene Electrodes for Stress Monitoring

Journal:	*Analyst*
Manuscript ID	AN-ART-10-2024-001389.R1
Article Type:	Paper
Date Submitted by the Author:	21-Nov-2024

Complete List of Authors:	Sharma, Atul; Tufts University, Department of Electrical and Computer Engineering; Tufts University School of Engineering, Tufts University Owyeung, Rachel; Tufts University Thomas, Ayanna; Tufts University School of Arts and Sciences, Department of Psychology Siraj, Sohel; Birla Institute of Technology & Science Pilani - Hyderabad Campus Keshari, Bishal; Birla Institute of Technology & Science Pilani - Hyderabad Campus, EEE Sahatiya, Parikshit; Birla Institute of Technology and Science - Hyderabad Campus Sonkusale, Sameer; Tufts University, Department of Electrical and Computer Engineering

SCHOLARONE™
Manuscripts

Please do not adjust margins

ARTICLE

Facile and Scalable Fabrication of Molecularly Imprinted Polymer (MIP) Sensors on Poriferous Laser-Engraved Graphene Electrodes for Stress Monitoring

Received 00th January 20xx,
Accepted 00th January 20xx

DOI: 10.1039/x0xx00000x

Atul Sharma [a,b], Rachel E. Owyeung [a,b], Ayanna Thomas [c], Sohel Siraj [d], Bishal Kumar Keshari [d], Parikshit Sahatiya [d], and Sameer Sonkusale [a,b*]

Monitoring cortisol levels is essential for understanding the body's response to stress. Traditional cortisol testing is confined to centralized labs, and current portable platforms are based on slow and complex assays. Here, we introduce a portable, disposable, non-invasive, and sensitive electrochemical sensor strip created using electropolymerized molecularly imprinted polymers (eMIPs) on laser engraved graphene (LEG) electrodes for rapid, simple, and reliable salivary cortisol detection. Herein, the characteristics of LEGs generated on a polyimide (PI) film with different laser processing parameters are also studied and optimized. The sensor quantifies salivary cortisol by selectively binding onto the cortisol-imprinted electropolymerized polypyrrole-Prussian blue (eMIP-PPy/PB) film on LEG electrodes. The PB redox probes embedded in the eMIP produce direct electrical signals upon cortisol binding, allowing sensitive and label-free amperometric detection. The developed cort-eMIP/LEG sensor strip displays an outstanding dynamic range (0.10 to 10,000 pg mL^{-1}), a remarkable limit of detection (0.08 pg mL^{-1}), and a strong correlation coefficient (R^2) of 0.9983 (n=4) for cortisol detection in human saliva. A rapid 3-minute analysis can more effectively measure cortisol levels in real-time than traditional methods. This sensor's performance was evaluated in human samples and validated two-way using enzyme-linked immunosorbent assays (ELISAs) and a third-party provider, Salimetrics, on 12 student volunteers exposed to varying stress levels. Results show an excellent correlation (r = 0.9948) between the developed sensors and standardized tests. The cort-eMIP/LEG cortisol sensor strip offers a simple, accessible, sample-to-answer diagnostic platform for stress monitoring.

Keywords: Saliva, Molecularly imprinted polymer, Laser-engraved graphene, Cortisol, Stress monitoring

Introduction

Monitoring and screening for stress-related health issues is crucial because prolonged exposure to stress can significantly impact both our physical and mental well-being [1–3]. The experience of distress varies from person to person and is influenced by a wide range of factors, including mental health, environment, medical history, and socioeconomic status. This complexity makes it challenging to assess its physical effects accurately [4]. Current diagnostic methods primarily rely on information provided by patients through psychological assessments and questionnaires, which can be subjective and inaccurate. In addition to these psychological evaluations, individual homeostasis to stress involves altering various physiological processes, leading to changes in biomarker levels (such as cortisol) that could potentially be used as markers for regular and on-demand screening [1,5]. This comprehensive approach promises a better understanding of the intricate relationship between emotional stress and its physical effects and the development of effective, long-term strategies for improving an individual's mental health with individualized therapies.

Cortisol (cort), a steroid hormone, is naturally released by the human body in response to both psychological and physiological stress. It plays a pivotal role in the body's stress response mechanisms and regulates metabolism and immune functions [2,6]. Elevated cortisol levels have been associated with an increased risk of conditions such as anxiety, depression, cardiovascular diseases, and compromised immune responses [5,7,8]. The cortisol secretion follows a circadian rhythm, increasing in the morning and gradually decreasing throughout the day. Furthermore, increased, or decreased cortisol levels than the normal range (morning: 10.2–27.3 ng mL^{-1} and evening: 2.2–4.1 ng mL^{-1}) [9], have been linked to the onset of Cushing's disease and Addison's disease [10,11], respectively. Given the importance of these findings, the development of efficient, rapid, and reliable cortisol detection methods holds significant value. Such advancements are essential for creating dynamic stress-response profiles, which can, in turn, support comprehensive therapy and wellness management [5,12–14]. Currently, clinical estimation of cortisol primarily relies on techniques such as fluorescent enzyme-linked immunosorbent assays (ELISA) [15], fluorometric assays [16], traditional liquid chromatography-tandem mass spectrometry (LC-MS) [15], radioimmunoassay (RIA) [16], and others. These methods are known for their high sensitivity and specificity to the analytes. Still, they are laborious, time-consuming, expensive, require large sample

[a] Sonkusale Research Lab, Halligan Hall, 161 College Ave Tufts University, USA;
[b] Department of Electrical and Computer Engineering, Tufts University, USA
[c] Department of Psychology, Tufts University, Medford 02155, MA, USA
[d] Department of Electrical and Electronics Engineering, BITS Pilani Hyderabad, Secunderabad, 500078, India
Corresponding author email: sameer@ece.tufts.edu
Electronic Supplementary Information (ESI) available: [details of any supplementary information available should be included here]. See DOI: 10.1039/x0xx00000x

Please do not adjust margins

volumes, and cannot be conducted in a point-of-care (POC) setting. Recently, point-of-care devices based on electrochemical sensors [17–19], surface plasmon resonance (SPR) sensors [20], and impedimetric biosensors [21] have been reported for the detection of cortisol. However, these technologies have several limitations, such as the need for mediators, complex electrode fabrication, a complex assay based on indirect cortisol measurement, high-voltage requirements, expensive instrumentation, or multi-step analyte modification to enable sensing. We are particularly interested in electrochemical approaches since they have shown excellent detection limits ranging from 1 pM to 1 µM, which can be further improved with better electrodes, recognition chemistry, and improved sample preparation and delivery [17,18,22].

Graphene, a two-dimensional material with high surface area and electrocatalytic activity, has attracted significant attention in biosensing and, more specifically, as an electrode for electrochemical sensing [23–27]. There are several graphene production methods, including chemical vapor deposition, chemical exfoliation, etc., [28], and thermal reduction of graphene [29,30]. Conventional methods require high-temperature processing or a multiple-stepped chemical synthesis, which lessens their widespread commercial potential. A straightforward and scalable approach uses a laser to write graphene and carbon nanostructures directly on polymeric substrates like polyimide (PI) thin films. Engraving is done using an infrared CO_2 laser, which results in laser-engraved graphene structures or LEG (it is also known as laser-induced graphene or LIG in some literature) [31–33]. In most cases, laser writing results in multi-layered graphene or carbon flakes. LEG or LIG have found widespread applications as electrodes for electrochemical sensors [34–36], batteries [37,38], and supercapacitors [32].

This work uses laser-engraving to produce poriferous laser-engraved graphene (LEG) with high porosity on polyimide (PI) films. The LEG method employs a CO_2 laser to directly pattern porous and multilayered graphene onto a thin PI surface. It is essential to optimize laser parameters such as laser power, exposure time, and PI thickness to obtain a very specific porous graphene realization of LEG, namely the LEG electrode. This is because photothermal (at high laser) or photochemical (at low laser) effects may affect the quality and composition of the LEG electrode [39]. Compared to simple graphene-based electrodes, LEG electrodes provide high surface area, better electrochemical activity, and higher sensitivity [40,41]. However, relatively few efforts have focussed on optimizing laser parameters to produce highly porous (or LEG) electrodes with further utilization in biosensing. In prior work, LEG-based electrodes were employed to sense cortisol. However, they used antibodies or aptamers as recognition elements [42,43]. While antibodies and aptamers provide high selectivity to cortisol, they are expensive, requiring multiple time-consuming steps to synthesize. Moreover, they are also sensitive to temperature and humidity and have a short shelf life. For this reason, artificial receptors based on electropolymerized molecularly imprinted polymers (eMIP), are more suitable since they are stable and can be synthesized faster in a low-cost manner. There is already a body of work on using MIP for selective recognition of salivary cortisol [12,44]. However, such MIP-based sensing commonly involves the use of external redox signalling probes, for example, ferrocyanide/ ferricyanide redox couple, which further limits their use as POC due to the need for sample and sensor preparation. Moreover, none of the prior methods have employed them for monitoring stress in a longitudinal study employing human subjects [12,44–46]. Such studies put more stringent requirements on sensor-to-sensor variability and demand scalability in fabrication. We show that there is potential for using LEG-based sensor strips to quantify human salivary cortisol levels with high sensitivity and selectivity and explore them for longitudinal studies for stress monitoring in human subjects with high reliability.

In this work, we develop a simple, facile, and scalable process to fabricate a portable and disposable LEG electrodes-based cort-eMIP sensor strip consistently and reliably on PI film. The LEG electrodes were prepared by CO_2 laser irradiating PI films in the atmosphere with optimal laser processing parameters (e.g., laser power, scanning speed, off-focus value, and scanning pass). The sensing approach is based on a label-free electrochemical approach, and the design consists of electropolymerized cortisol (cort) binding MIPs, namely cort-eMIPs as cort receptors. Fabrication of the platform involves a one-step, rapid, reproducible synthesis of a cort-receptor sensing membrane that begins with the direct electropolymerization of polypyrrole (PPy) in the presence of Prussian blue (PB) as embedded redox couple and cort as template molecules on surface activated LEG electrode. Subsequently, the elution of cortisol from the cort-eMIP membrane was achieved via overoxidation of PPy-PB film, which induces a structural change in the polymer that releases the template cortisol molecule and leaves cort-binding sites inside the matrix. This obviates the need for complex labelling procedures or external redox probes. Different PPy-PB stochiometric ratios, electropolymerization cycles, pH effect, and monomer–template ratios were tested to optimize the cort-eMIP/LEG sensor performance. Interactions such as hydrogen bonding (H-bonds) and electrostatic forces are essential in releasing or re-binding the target analyte on the cort-binding site. The resulting platform consists of cort-eMIP on a single-use LEG-electrode with companion compact read-out electronics for an on-demand and easy-to-use stress monitoring anytime and anywhere. To demonstrate the applicability of this cort-eMIP sensor platform, we deployed them to monitor cortisol levels in human saliva samples collected as part of a stress study from 12 student volunteers exposed to different stress levels. To the best of our knowledge, this is the first report where a LEG-based cort-eMIP sensor has been used reliably for longitudinal stress monitoring in human subjects. The reliability, as shown by the coefficient of variance of less than 8%, and sensitivity demonstrated by the LOD is less than 0.08 $pgmL^{-1,}$ representing a significant advance in salivary cortisol detection from a point-of-care (POC) diagnostic platform.

Materials and Methods

Materials and Reagents

Pyrrole (98%), potassium chloride (KCl), hydrochloric acid (HCl, ACS reagent 37%), potassium ferricyanide [$K_3Fe(CN)_6$], iron chloride hexahydrate ($FeCl_3.6H_2O$), sodium dihydrogen phosphate (NaH_2PO4), disodium hydrogen phosphate (Na_2HPO_4), and sodium chloride (anhydrous) were all purchased from Sigma Aldrich and used as received. Methanol (99%) was purchased from Thermo Scientific and used as received. Cortisol was purchased from Sigma Aldrich and used as received. The cortisol competitive human ELISA kit was procured from ThermoFisher Scientific, USA. All the solutions were prepared in 0.20 µm membrane-filtered deionized water. Polyvinyl butyric acid (PVB, Butavar (B-98) was procured from Benton Chemical, USA, and used as received. The silver/silver chloride (Ag/AgCl) conductive ink for coating connection pads was procured from Kayaku Advanced Materials (USA). A polyimide sheet (PI) of 1.0

 This journal is © The Royal Society of Chemistry 20xx

cm x 1.0 cm was layered on a polyethylene terephthalate (PET) substrate to fabricate the LEG-electrode. The PI (thickness 12.5 µm) was procured from Grainger, USA, and used as received. Testosterone, corticosterone, glucose, and lactate were purchased from Sigma Aldrich (USA) for interferent studies.

Instrumentation

A laser engraving and cutting system, equipped with a CO_2 laser of wavelength λ = 10.6 µm, was employed to fabricate LEG under various conditions. These conditions involved the variation of laser power (P), scanning speed (v), repeated scanning passes (n), off-focus value (Δf), image resolution, and gas flow. The surface morphology of the fabricated sensor at different stages was characterized using Nicolet 6700 FTIR attached with Smart iTX (Thermo Scientific) in ATR mode. Raman spectrum was recorded on a DXR Raman microscope (Thermo Scientific) at 532 nm. Scanning electron microscope (Axia), Thermo Scientific, USA, used to generate SEM images. The potentiostat used (Electrochemical Workstation), and the commercial Ag/AgCl reference electrode were purchased from CH Instruments. The phase and structural identification of the grown Graphene oxide was done by X-ray diffraction method (RIGAKU ULTIMA-IV instrument with Cu-Kα X-ray source). Thermo Scientific Multilab 2000 with Al Kα radiation operated at 15 kV, XPS instrument was utilized to identify Fe and N doped graphene oxide material's elemental composition and oxidation states. Further deconvolution of overlapped peaks identifies the chemical compositions of each element for each sample. Furthermore, their adjusted peak areas calculated the accurate atomic percentage of each composition present in the matrix.

Fabrication of LEG electrodes

The LEG electrodes, comprising a 3-electrode system, were fabricated using a laser ablation technique on a PI sheet (see Fig. S1). Among the three electrodes, the middle one was designated as the working electrode (WE), while the curved one was defined as the counter electrode (CE). The third electrode was coated with Ag/AgCl paste and then baked at 60°C for 1 hour. Subsequently, the reference electrode was established by drop-casting a PVB-membrane cocktail (consisting of PVB polymer containing sodium chloride dissolved in methanol) onto the Ag/AgCl-coated electrode to designate it as a reference electrode (RE). Before use, the LEG electrodes were activated with 0.50 M H_2SO_4 (containing 0.10 M KCl) by sweeping the voltage between 1.0 and -1.20 V at a scan rate of 100 mV/ sec (5-6 cycles) until a flat CV curve was obtained (data not shown). This step ensures the surface is thoroughly cleaned and ready for further use.

Fabrication of cort-eMIP sensor

The fabrication of the cort-eMIP sensor was carried out through electropolymerization using cyclic voltammetry (CV) within a potential range of -0.30 to +0.80 V, with a scan rate of 50 mV/s, for 20 cycles in phosphate-buffered saline (PBS) with a pH of 7.4. The polymerization solution contained pyrrole (6.0 mM), cortisol (1.5 mM), $FeCl_3.6H_2O$ (5.0 mM), $K_3[Fe(CN)_6]$ (5.0 mM), and HCl (0.10 mM) until optimized. Following electropolymerization, the cort-eMIP electrode underwent three washes with PBS to remove any unreacted compounds. The embedded cortisol molecules were extracted from the PPy-PB matrix through over-oxidation by sweeping the potential from -0.40 to +0.60 V for 20 cycles in PBS to create specific binding sites for cortisol. The non-imprinted polymer, referred to as the cort-eNIP electrode, was fabricated similarly, except that no template (cortisol) was included in the polymer cocktail mixture.

Human saliva collection and storage

All samples were obtained using the Tufts University Institutional Review Board (IRB) approved protocol under Protocol No. 1706030. Human saliva samples were collected from student volunteers at Tufts University using validated polypropylene vials, specifically SalivaBio 2ml cryovials (Salimetrics Item No 5004.01), through the passive drooling method. The collection occurred at four distinct time points (baseline, immediate pre-stress, immediate post-stress, and 20 min post-stress) to investigate the stress response. After collection, the vials were securely sealed to withstand temperatures as low as -80 °C They featured external threading to facilitate the use of the Saliva Collection Aid (SCA- Salimetrics Items No. 5016.02) for guiding drool directly into the cryovial. Participants inserted a small cotton tube into their mouths and sucked on it for one minute, then placed the cotton piece into a tube for later testing. Subsequently, the tubes were transferred to a conical tube storage box and stored in a laboratory refrigerator set at -80 °C for preservation. All salivary cortisol underwent testing using the enzyme-linked immunosorbent assay (ELISA), a standard testing method, within three months of collection. Samples were shipped frozen to Salimetrics for ELISA analysis via FedEx. The saliva collected from the bottom of the V-tube underwent further testing with the Cort-sensor and a commercial cortisol ELISA-Kit.

Matrix (Human Saliva) preparation for cortisol detection

The saliva sample obtained from the lower part of the salivary vessel was subjected to centrifugation at 2500x rpm for 20 minutes. The resulting supernatant was collected, mixed with an equal volume of PBS (at a 1:1 ratio, v/v), and thoroughly homogenized before usage. A 20 µL aliquot of the saliva sample was applied to the electrode surface for cortisol sensing. At the same time, the second portion was utilized for cortisol ELISA-kit testing to validate the results. The dilution factor was considered when determining the actual concentration of cort in the saliva sample. After the testing, the sensors and materials that had encountered the saliva samples were handled in compliance with regulatory guidelines to mitigate potential biohazard risks.

Sensor readout using Chronoamperometry (CA)

To emphasize the interfacial properties of the fabricated cort-eMIP sensor at each fabrication step, the CV and differential pulse voltammetry (DPV) were performed in 0.10 M PBS (pH 7.4, containing 0.10 M KCl as electrolyte) buffer. The sensor sensitivity was measured using chronoamperometry (CA) to measure the change in the oxidation current of PB on the electrode surface after cortisol occupied the memory sites. A 20 µL specific concentration of cortisol prepared in PBS was dropped on a horizontally supported three-electrode surface. Post incubation (2 min), the CA was applied under the following conditions: initial potential 0 V, a high potential 0.10 V for a pulse width of 60 sec with a sample interval of 0.10 sec. Change in oxidation current was measured post stabilization of signal after 40 sec vs. Ag/AgCl.

Results and Discussion

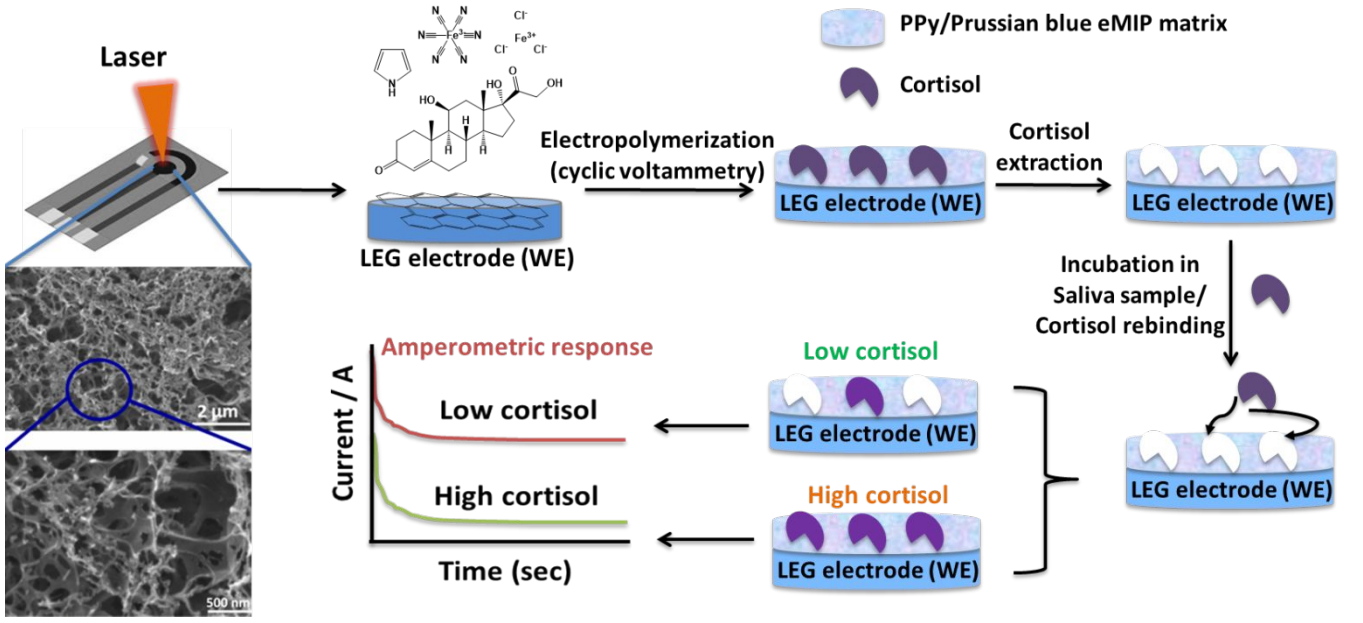

Figure 1: Schematic for fabrication of Cort-eMIP sensor (eMIP- electropolymerized molecularly imprinted polymer; CV- Cyclic voltammetry; Cort-Cortisol; RE- reference electrode; PBS- phosphate buffer saline).

Sensor design and principle

The proposed cort-eMIP sensor relies on amperometric transduction, utilizing the Cort-PPy-MIP layer to detect cortisol molecules. Fig. 1 illustrates the schematic representation of the Cort-eMIP/LEG sensor, which incorporates a three-electrode system (working electrode-WE, counter electrode-CE, and reference electrode-RE). These electrodes (WE, CE, and RE) have been integrated into a PI film through laser engraving. The WEs have been created by optimally carbonizing PI, resulting in a multilayer and porous graphene structure at the engraving site. Subsequently, one of the three electrodes is coated with Ag/AgCl ink to convert into an RE. For WE, Cort-PPy-MIP is polymerized on one of the LEG electrodes through the electropolymerization of polypyrrole (PPy) on an electrochemically activated LEG electrode. The oxidation of pyrrole (as a functional monomer) in a cocktail solution containing cortisol (as a template) with ferric trichloride and ferricyanide resulted in the formation of the embedded PB-redox mediator and the creation of Cort-PPy-eMIP. The PPy-LEG layer provides a highly conductive surface and receptor loading, while eMIP offers a high binding affinity. These properties further enhance sensitivity. The subsequent step involved the extraction of cortisol molecules from the scaffold, achieved through the over-oxidation of pyrrole. This process led to the creation of molecularly imprinted cavities within the PPy-film. Cort-PPy-eNIP was prepared similarly but without cortisol molecules in the cocktail solution. In the presence of cortisol as the template, cortisol molecules diffused into these cavities, binding within the memory sites/ pockets and creating a barrier to electron transfer. For WE, the cort-eMIP film is meticulously grafted onto its LEG surface. This film strip with three electrodes is then used for chronoamperometric (CA) measurements for cortisol quantification in target media, as depicted in Fig. 1.

Fabrication of Cort-eMIP/ eNIP films

Pyrrole monomers can be electro-oxidized to enable the controlled formation of PPy-matrix onto a transducer surface by applying a potential [47]. Several parameters influence the growth of the polymer matrix [48]. For instance, high monomer concentrations are known to reduce the eMIP sensitivity due to the formation of films with excessive density or thickness, leading to insufficient binding sites [47]. Non-optimized crosslinkers and template stoichiometric can lead to loosely bound eMIP, which might result in degradation and lower binding affinity [49,50]. To address the above concerns, we employed CV to control the oxidation process, following an earlier reported method with optimized electrodeposition parameters [7]. Fig. 2a and 2b shows the voltammograms generated from the electropolymerization of cort-eMIP and cort-eNIP on the LEG electrode surface, respectively. To act as a control for comparison with the eMIP sensor, the eNIP sensor is prepared similarly but without adding a template molecule to the cocktail solution. As the eMIP film is electropolymerized and growing onto the electrode, the cortisol molecule diffuses through the precursor mixture and becomes embedded in the resulting film, whereas eNIP does not contain cortisol molecules. Fig. 2(a) shows how, from -0.30 to 0.80 V (the region encircled with the dotted line), the magnitude of the oxidation and reduction peak current signal increases in the direction the arrow indicates as the film grows. The behavior is also observed for the NIP film (Fig. 2b), but there is no significant change in the current intensity or an increase in film thickness when compared to eMIP film formation. It is plausibly due to the lack of formation of a polymeric layer with the absence of an electroactive cortisol molecule [51]. A negligible increase of current signal after 20 electropolymerization cycles (Fig. 2a and 2b) signifies that the electrode surface is covered with eMIP film of sufficient thickness, where further electropolymerization cycles might be counterproductive as it will generate a thicker polymeric film limiting charge transfer from the electrode surface through the eMIP film, which will lead to the lower sensitivity [51,52]. Therefore, a 20 CV deposition cycle was selected to fabricate the eMIP and eNIP films.

The next step involved extracting bound cortisol-template molecules from the eMIP scaffold to create complementary or memory sites. During the polymerization process, the following

 This journal is © The Royal Society of Chemistry 20xx

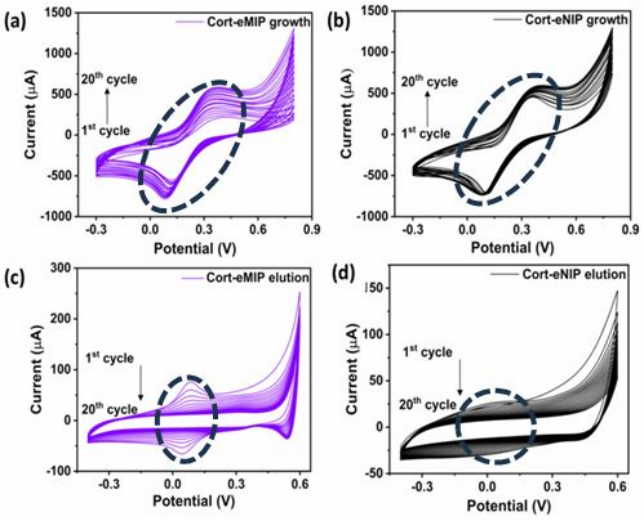

Figure 2: Cyclic voltammograms of (a) eMIP deposited in the polymeric cocktail containing (pyrrole-6.0 mM, cortisol- 1.5 mM, $FeCl_3.6H_2O$ -5.0 mM, $K_3[Fe(CN)_6]$-5.0 mM, and HCl -0.10 mM and (b) eNIP deposited without template at the potential range of -0.30 to +0.80 V, with a scan rate of 50 mV/s, for 20 cycles in phosphate-buffered saline (PBS) with a pH of 7.4 Cyclic voltammograms of (c) cortisol elution from eMIP and (d) eNIP matrix by at potential range of -0.40 to +0.60 V, with a scan rate of 50 mV/s, for 20 cycles in phosphate-buffered saline (PBS) with a pH of 7.4.

interactions could occur (i) hydrogen bonding interaction between the hydroxy group of cortisol and the imide nitrogen of PPy, and (ii) hydrogen bonding interaction between the carboxy group of cortisol and the imide nitrogen of PPy [47,51]. Voltammetric overoxidation of the PPy scaffold results disrupts the hydrogen bonding interaction, allowing cortisol to be eluted and generating complementary cavities of cortisol in the eMIP film [47,51]. We employed overoxidation in a buffer solution to prevent damage to the MIP layer. By applying the appropriate electrode potentials, overoxidizing the pyrrole-MIP layer improved the selectivity and sensitivity of PPy-based MIP sensors, resulting in superior selectivity for the imprinted analytes [53,54]. Additionally, removal of template molecule by overoxidation, as opposed to extraction by washing with organic solvents, helps avoid solvent-induced swelling of the PPy/PB scaffold, which could promote nonspecific binding [55]. The elution process was performed in a PBS buffer.

As depicted by the directional arrows in Fig. 2c and 2d, this process resulted in a decrease in current magnitude in response to an increasing number of CV elution cycles, as weakly bound pyrrole and redox precursors were removed during film conditioning, and as cortisol emerged from the eMIP film (Fig. 2c). The elution of the eNIP film (Fig. 2d) showed a lack of cathodic and anodic peak in current magnitude, indicating that the elution process caused irreversible oxidation of the PPy/PB scaffold. From Fig. 2c, it is evident that there was no significant difference in the magnitude of sensor current after 15 cycles. This suggests that 15 elution cycles could be sufficient. However, 20 cycles were selected to ensure the effective conditioning of the eMIP film. The prepared sensors were stored at room temperature under a nitrogen environment if not in use.

Characterization and analytical performance

Surface characterization

The LEG electrode was fabricated by optimizing different laser parameters (power, speed, focus, and direction), as summarized in the supplementary section (ST1). The laser power of 22 with a laser

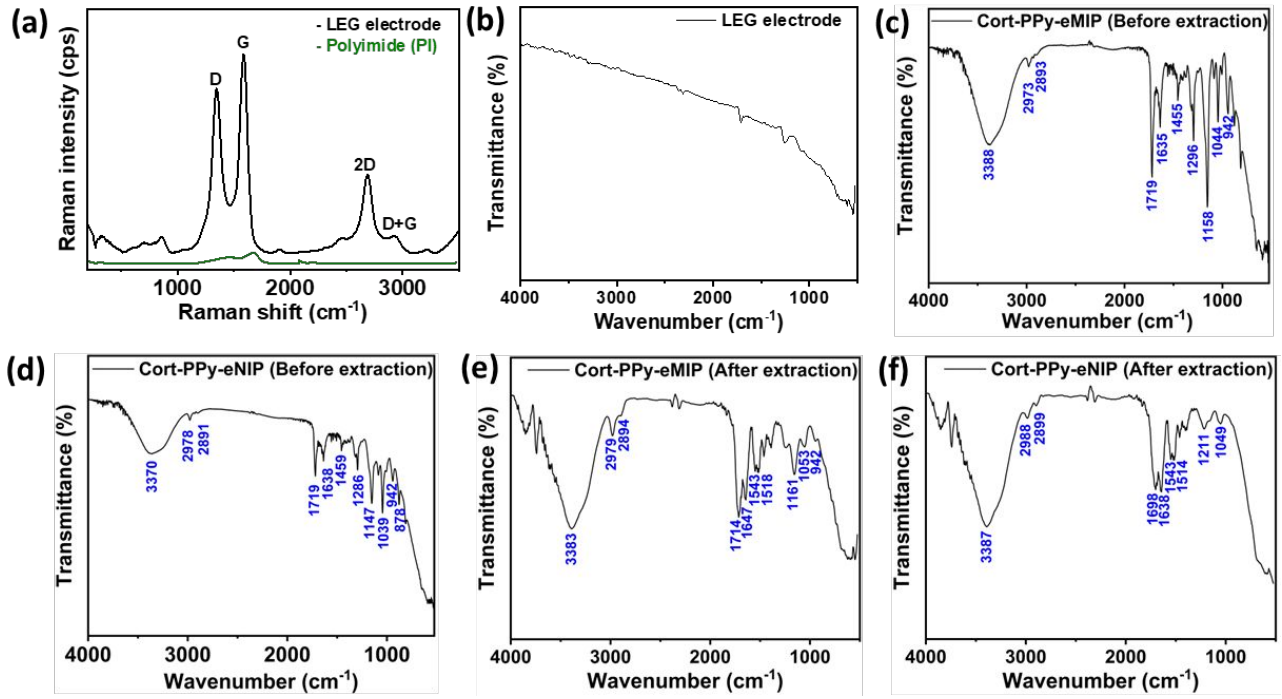

Figure 3: (a) Raman spectrum of LEG-electrode (black curve) and polyimide (PI, green curve); FTIR spectrum of (b) LEG-electrode; (c) before extraction of electropolymerized Cort-eMIP on LEG electrode; (d) before extraction of electropolymerized Cort-eNIP on LEG electrode; (e) after extraction of electropolymerized Cort-eMIP on LEG electrode; (f) after extraction of electropolymerized Cort-eMIP on LEG electrode at a scan rate of 32 cm^{-1} in ATR mode.

speed of 5.25 % with 0.50 mm defocus resulted in the desired LEG electrode for this application. The resulting LEG electrodes exhibit an average resistance of 32 ± 5 Ω/cm (n = 6). The Raman spectrum of the porous laser-engraved graphene (LEG) electrode and polyimide (PI) surface were compared to study and confirm the graphene production. The Raman spectrum of the LEG electrode exhibited three distinguished peaks (D, G, and 2D peaks) (Fig. 3a, curve a). In contrast, the non-engraved PI surface did not show any prominent band (Fig. 3a, green curve), which is usually present within 1200-1300 cm^{-1}. Small spikes close to the baseline between 1800 to 2500 cm^{-1} are due to the background signal. This observation is consistent with findings reported in the literature by Lin et al. and others [28,32]. The D peak (roughly at 1,356 cm^{-1}) is reflected by either sp^2 bonds between atomic carbons or lattice defects, and a second peak, a G peak roughly at 1,586 cm^{-1}, appeared. The third and second-order D (2D) peak is unique to randomly stacked graphene sheets in the c-axis [32,56] and was observed at roughly 2714 cm^{-1}. Ultimately, the intensity ratio of the D/G confirms the extent of graphene formation during the LEG fabrication process. In Fig. 3a, the ratio of 2D/G peaks is calculated as 0.66, indicating the formation of multilayer graphene structures (n = 10). The FT-IR spectrum in Fig. 3b-f shows a characteristic signal peak corresponding to the formation of cort-eMIP or cort-eNIP. In Fig. 3c, the LEG electrode lacks prominent vibrational peaks associated with IR-inactive functional groups, such as (-OH, -C=O, -COOH), typically observed in graphenic material [57]. This suggests a low level of defects in the graphene polyimide. The cort-eMIP showed vibrational bands corresponding to the PPy ring in the fingerprint's region at 1635, 1455 cm^{-1} for cort-eMIP and 1638, 1459 cm^{-1} for eNIP. The blue shift in eNIP signifies the absence of electrostatic interaction between the cort and PPy polymeric chain. The presence of additional bands at around 2850-3000 cm^{-1} (due to -CH stretching vibrations) with the medium band at 1044 cm^{-1} (cort-eMIP) and 1039 cm^{-1} (cort-eNIP) confirm the formation of the PPy network. Cortisol-bound eMIP showed strong peaks around 1719 cm^{-1} (str, -C=O) and 1158 cm^{-1} for -CN vibration with an out-of-plane bending vibrational at 942 cm^{-1} complement to broad peak centered around 3388 cm^{-1} due to hydrogen-bonded -OH stretching of cortisol [44,58,59]. Post extraction, the signal around 1147 cm^{-1} and 942 cm^{-1} are almost disappearing in cort-eMIP and absent in cort-eNIP, which resembles the absence of hydrogen bonding and confirms the cortisol is being completely extracted from eMIP.

The X-ray diffraction (XRD) studies for the base electrode, e-NIP with extraction, e-NIP without extraction, and e-MIP with extraction are presented in Fig. S2, revealing the characteristic crystal structures of these samples. The (002) reflection plane peaks appear at 2θ values of 22.82°, 22.92°, 22.87°, 22.93°, and 22.91°, respectively, indicating a consistent interlayer arrangement across the samples. For comparison, graphene displays a distinct (002) peak at 2θ = 26.5°. The shift in interlayer spacing observed in the samples suggests the intercalation of oxygen-containing groups, which disrupted the original crystal structure. This modification likely results from the oxidation occurring during the reduction of polyimide to graphene.

X-ray Photoelectron Spectroscopy (XPS) is a powerful technique for characterizing the MIP in sensors [60–62]. XPS measurements were performed on each step of the sensor fabrication procedure. XPS signals originating from C, O, N, and Fe atoms within the film are measurable on the respective samples. Fig. 4a, the wide-scan spectrum shows multiple peaks corresponding to the elements in the electrochemically treated laser-engraved graphene electrode with C and O. In Fig. 4b-4c, the XPS signatures at binding energy ~284.8 eV and 532 eV corresponding to C1s and O1s were observed as expected for graphene-based materials [63–65]. As shown in Fig. 4d and 4e, the peaks for C 1s, O 1s, N 1s, and Fe 2p are evident, confirming the successful doping of nitrogen and iron in the material during the electropolymerization process [63,65]. The appearance of C 1s (~284 eV), N 1s peak (~400 eV), Fe 2p peak (~711 eV), and O 1s peak (~530 eV) confirms the successful introduction of nitrogen and iron atoms into the structure [66]. Fig. 4f displays the deconvoluted C 1s spectrum, indicating the different bonding states of carbon, representing the intact graphene structure for bonded to nitrogen or oxygen (C–C, C–N, C–O) [64], typical in graphene-based materials [6]. Similarly, Fig. 4g shows peaks corresponding to different oxygen functionalities on the functionalized electrode surface. The peak at 531.6 eV is assigned to carbonyl oxygen (C=O) or metal-oxygen bonds (M–O, where M is iron) [66]. The peak at 532.2 eV is attributed to the C–O bond, and the peak at 533 eV corresponds to oxygen in hydroxyl (C–OH) or epoxy (C–O–C) groups [67]. Fig. 4h shows a peak around 400 eV attributed to pyrrolic nitrogen, where nitrogen is bonded to two carbon atoms within a five-membered ring [65]. The peak at 401 eV is associated with graphitic nitrogen, indicating nitrogen incorporated into the graphitic plane [68]. The high-resolution Fe 2p spectrum (Fig. 4i) reveals several distinct peaks, indicating the presence of iron oxidation states [66,69]. Similar findings were obtained for the cort-eNIP electrode (Fig. S3, without template extraction), cort-eMIP electrode before template extraction (Fig. 4j and Fig. S4), and cort-eMIP sensor electrode after template extraction (Fig. 4k-4o) procedures.

Apart from the positioning of peaks in the XPS spectrum, it is important to compare the atomic ratio to evaluate the estimate of the removal of cortisol after extraction. The atomic ratio between N1S (pyrrolic) and O1S has been used to quantitively estimate template removal after overoxidation of the sensor in a buffer medium. In particular, the atomic ratio decreases from 1.13 ± 0.03 to 0.92 ± 0.02, confirming the removal of cortisol during overoxidation in buffer medium, as already observed in SEM and CV (overoxidation) analyses. The energies and assigned chemical groups for each peak within the region's envelopes are listed in ST2. All the features in cort-eNIP are present in the cort-eMIP sensor before and after the cortisol extraction procedure; the only noticeable difference can be found for C=O/Fe-OH percentage, which decreases post-extraction. This is due to removing cortisol molecules bearing C=O and C-O functional groups. If the component relative to Fe on the MIP before and after template removal are compared, it is possible to observe that its intensities increase after overoxidation in buffer, possibly due to the removal of cortisol and its oxygen functional groups. It is important to note that the same component did not increase in the cort-eNIP film when treated in a buffer medium. This confirms that the adopted process was reliable enough to fabricate the MIP-based sensor.

This journal is © The Royal Society of Chemistry 20xx

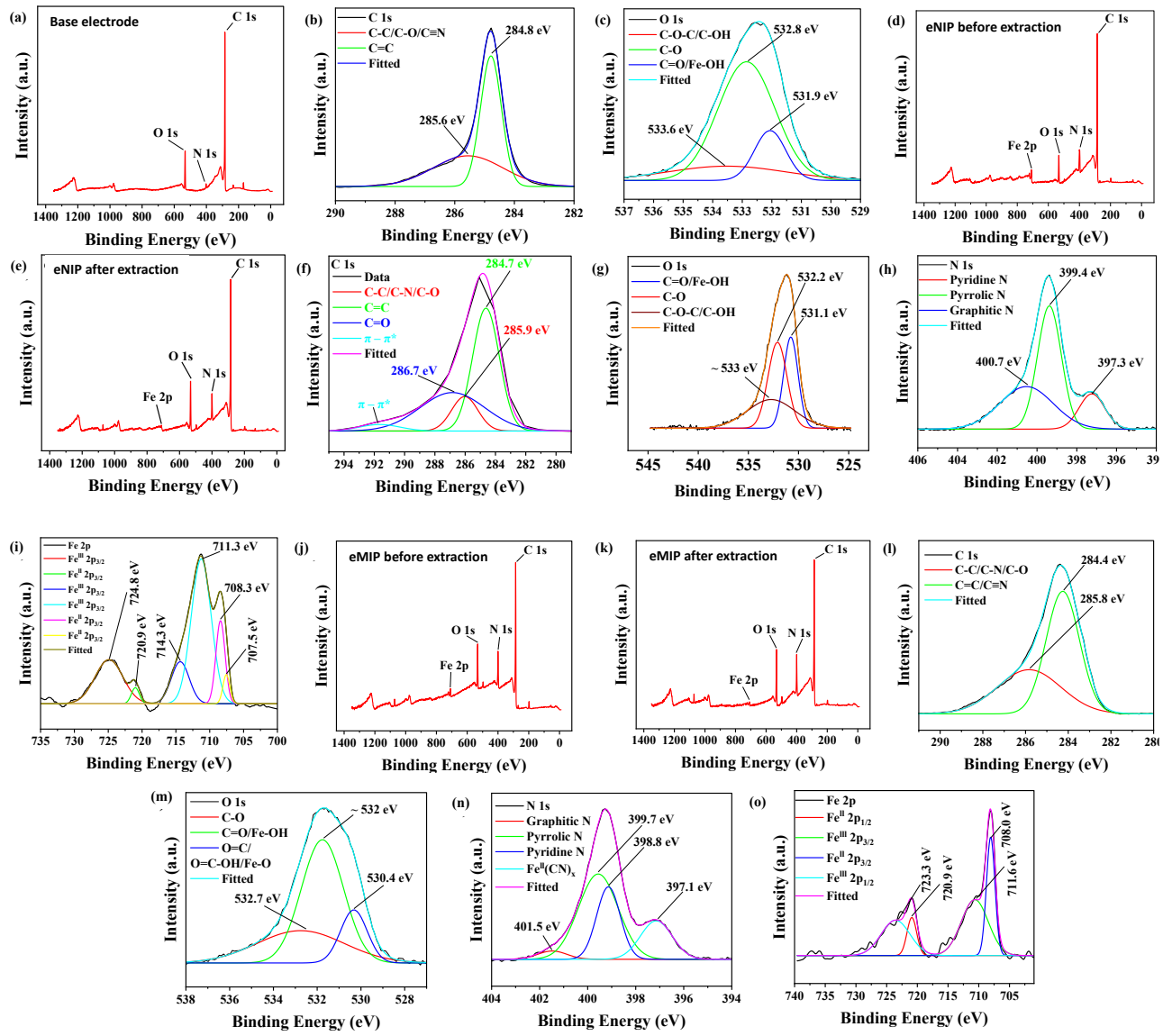

Figure 4: High-resolution XPS survey and deconvoluted spectra for (a-c) bare electrode; (d) e-NIP electrode without and (e-i) after cortisol (template) extraction; cort-eMIP electrode (j) before extraction and (k-o) after cortisol extraction.

In Fig. 5, the scanning electron microscopy (SEM) studies reveal the surface morphology of the LEG electrode (Fig. 5a-c), and how it changed after each modification step on the LEG (Fig. 5d-f). A highly network and multilayer porous graphene can be easily seen in Fig. 5a. Fig. 5b and 5c represent the zoom-in image depicting the porous LEG surface. The cort-eMIP electrode surface is covered with polymeric film post-electropolymerization (Fig. 5d). The comparison between template-bound eMIP and eNIP films suggests that the eNIP electrode develops non-porous surface morphology compared to eMIP. This could be due to the presence of cortisol in eMIP while eluting, leaving a porous structure behind, as evident from Fig. 5e. In contrast, eNIP film grows with a lack of cortisol molecules (Fig. 5f), enabling polymerization to process through more extended branch-like formations. The surface roughness of the modified working electrodes was assessed using atomic force microscopy (AFM). This technique provides detailed surface topography analysis, including two-dimensional (2D) and three-dimensional (3D) images, as shown in Fig. S5. Fig. S5a presents the cort-eNIP electrode surface formed by electropolymerization. The roughness was quantified using the root mean square (RMS, R_q), which was 1.074 ± 0.330 µm (R_{sk} = -0.0143) for the cort-eNIP electrode respectively. Before template removal, the R_q value increased to 2.059 ± 0.249 µm (R_{sk} = -0.0286) for the cort-eMIP electrode, likely due to cortisol entrapment within the polymeric scaffold. After template extraction, further topographical analysis revealed a significant increase in R_q value, indicating a substantial rise in surface roughness attributed to the formation of cavities. The R_q value for the cort-eMIP electrode (post-template removal) was 2.524 ± 0.196 µm (R_{sk} = -0.0258). The negative skewness, indicating surface asymmetry, supports the presence of cavities after template extraction. The obtained results are well aligned, as reported in the literature [60,62]. Furthermore, one

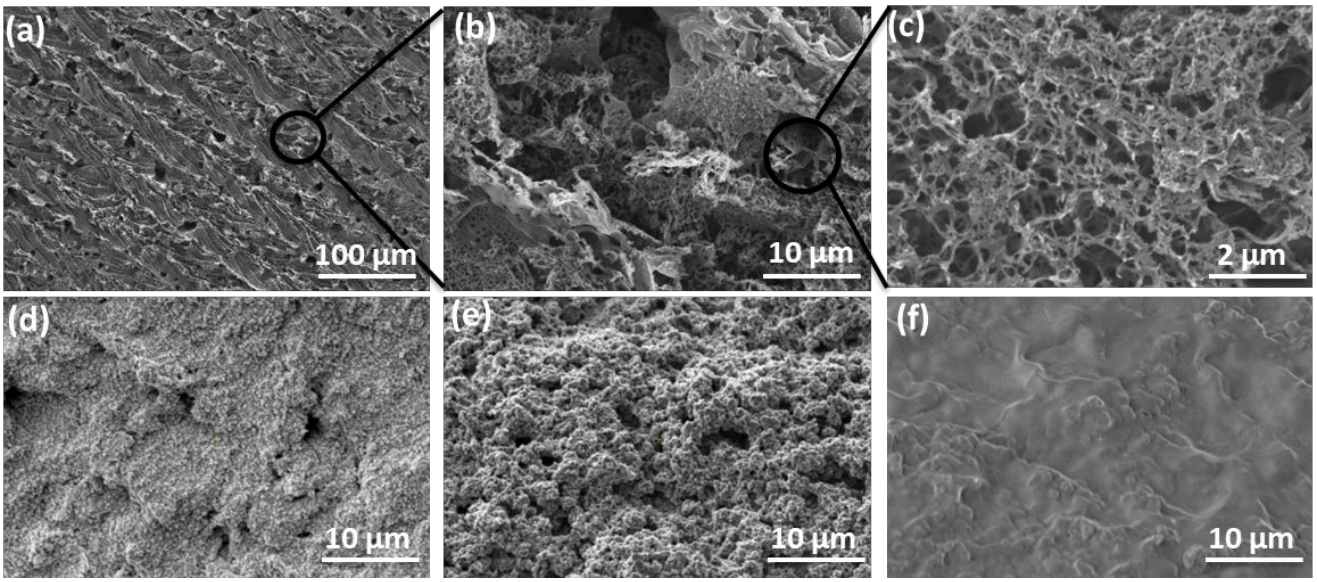

Figure 5: SEM images of (a) cleaned LEG-electrode (at 100 µm); (b) zoom-in image of LEG-electrode (at 10 µm); (c) LEG-electrode (at 2 µm); (d) cort-eMIP electrode before extraction (at 10 µm); (e) cort-eMIP electrode after extraction (at 10 µm); (f) cort-eNIP electrode after extraction (at 10 µm).

might be interested in performing a Brunauer-Emmett-Teller (BET) surface area analysis. This could allow measurement of the surface area and pore size distribution of electropolymerized MIP and will help in studying in detail the cavities formed from eluting the bound template [70]. This was not the focus of this study, as characterization studies employed confirmed the surface morphology [60,62,71].

In Fig. S6a, the CV study demonstrates the sensor response at different scan rates ranging from 10 to 500 mV/s. The CV analysis revealed a quasi-reversible process observed at a slower scan rate. The oxidation and reduction peaks depicted in the CV (Fig. S6a) show a relatively equivalent potential response. As the scan rate increased, the peak current increased, indicating steady electron transfer kinetics on the sensor strip surface. Furthermore, the oxidation and reduction currents exhibited a linear increase with the square root of the scan rate (Fig. S6b). This suggests electrochemically reversible electron transfer processes involving freely diffusing redox species, closely matching the Randles–Sevcik equation.

Optimization and analytical performance

Fig. 2c shows that the cort-eMIP sensor, fabricated through electropolymerization/ elution, displays an oxidation peak around 0.10 V. This peak can be attributed to the PB redox mediator embedded in the eMIP scaffold. To investigate this further, eMIP sensors were subjected to CV measurements in PBS at a concentration of 0.10 M and a pH of 7.4, both with and without cortisol concentrations (1.0 pg mL^{-1}). The results obtained in Fig. 6a (DPV) and 5b (CV) reveal that an increasing cortisol concentration causes a decrease in the magnitude of the oxidation peak current signal around 0.10 V. This reduction is attributed to cortisol diffusing from the solution into unoccupied cavities within the cort-eMIP scaffold, which acts as binding sites. In contrast, the cort-eNIP sensors did not exhibit any similar changes. The bound cortisol molecules hinder the charge transfer or PB oxidation, resulting in a decrease in current. Based on these findings, the current signal (CA) was measured at a fixed potential of 0.10 V across a series of eMIP sensors with 60 µL of cortisol solutions in PBS at varying concentrations (ranging from 0.10 to 10000 pg mL^{-1}).

The chronoamperogram displayed in Fig. 6c shows an apparent stabilization of the current signal after approximately 60 seconds, governed by diffusion [72]. Therefore, the signal at 60 seconds for each cortisol concentration was used to establish a calibration curve. The resulting graph (Fig. 6c) illustrates a decrease in the eMIP current signal with an increase in cortisol concentration from 0.10 to 10000 pg mL^{-1}. The cort-eNIP sensor did not significantly change in the current with increased cortisol concentration (Fig. 6d). Fig. 6e and 5f show the magnified chronoamperogram for the eMIP and eNIP cort sensor, respectively. The sensors' sensitivity within the 0.10 to 10000 pg mL^{-1} cort concentration range is 0.8518 µA log^{-1} (pg mL^{-1}), with a coefficient of correlation (R^2) of 0.9844 for n=4 sensors at each concentration (Fig. 6g). The limit of detection (LOD) was calculated from the regression equation in Fig. 6g, using the average standard deviation (SD) and slope, where LOD = (3.3 x SD) / slope, resulting in a LOD of 0.08 pg mL^{-1}. The relative reproducibility over four sensor sensing strips for each concentration was also calculated. The high precision is further demonstrated in Fig. 6h, where chronoamperometric measurements obtained from four sensors at cortisol/PBS concentrations of 0.0 and 10 pg mL^{-1}, with a sensor current at 60 seconds, present relative standard deviations (% RSD) of 3.29%, and 2.69 %, respectively are presented.

A series of incubation times were tested to optimize the optimal time required to allow the diffusion of cortisol molecules from the test solution into the eMIP sensor strip cavities. Fig. S7 demonstrates that the measured current from sensors incubated in 60 µL of 1.0 pg mL^{-1} cortisol for 1, 2, 5, 7, and 10 min. The change in current did not change much after 2 min of incubation. Therefore, the 2-minute incubation time was used as the optimum time, which provided a rapid measurement time of 3 minutes, including a 1.0-minute measurement time. The saliva pH may vary in each individual based on their diet and health status. This suggests that pH might affect sensor performance. To investigate this, measurements were performed in 1.0 pg mL^{-1} cortisol at pH levels of 6, 6.5, 7.0, 7.4, and 7.8, covering the physiological range of human saliva. The results

 This journal is © The Royal Society of Chemistry 20xx

(Fig. S8) confirm that the maximum change in current was observed at pH 7.4. Therefore, pH 7.4 was used in further experimentation. Fig. S9 and S7 show the effect of monomer and template-monomer ratio. It is evident from Fig. S9 (monomer concentration) and Fig. S10 that the monomer: template ratio of 2:1 and 4:1 showed similar responses. This higher response could be attributed to the optimum polymer matrix network (PPy-PB) with maximum interaction with template (cortisol) molecules. However, to maximize and achieve higher binding efficiency, a 4:1 (pyrrole: cortisol) ratio was selected and used in further experimentation (Fig. S10).

The developed sensor is specifically designed to analyze human saliva samples, representing intricate compound mixtures. Saliva contains various small molecules, including hormones that bear structural similarities to cortisol, such as testosterone, glucose, lactate, etc. These analogous molecules can potentially disrupt the sensor's performance by binding to the eMIP cavities, thereby altering the sensor's signal. To assess the cort-eMIP sensor's specificity, we conducted current response measurements across a spectrum of potential structural and non-structural interferents at concentrations relevant to physiological conditions. Fig. 6i depicts the current responses that were obtained from interference experiments. Our findings indicated that these potential interferents induced a significantly smaller deviation in the current (less than 10%) compared to the sensor's response to the cortisol target (at 1.0 pg ml^{-1}). The current response observed during cross-reactivity could be derived from the unwanted interaction of interferents with hydroxyl groups, resulting in interaction or somehow trapped due to their small size, such as glucose. Furthermore, a control experiment employing cort-eNIP sensor strips (depicted in Fig. 6d and 5g)

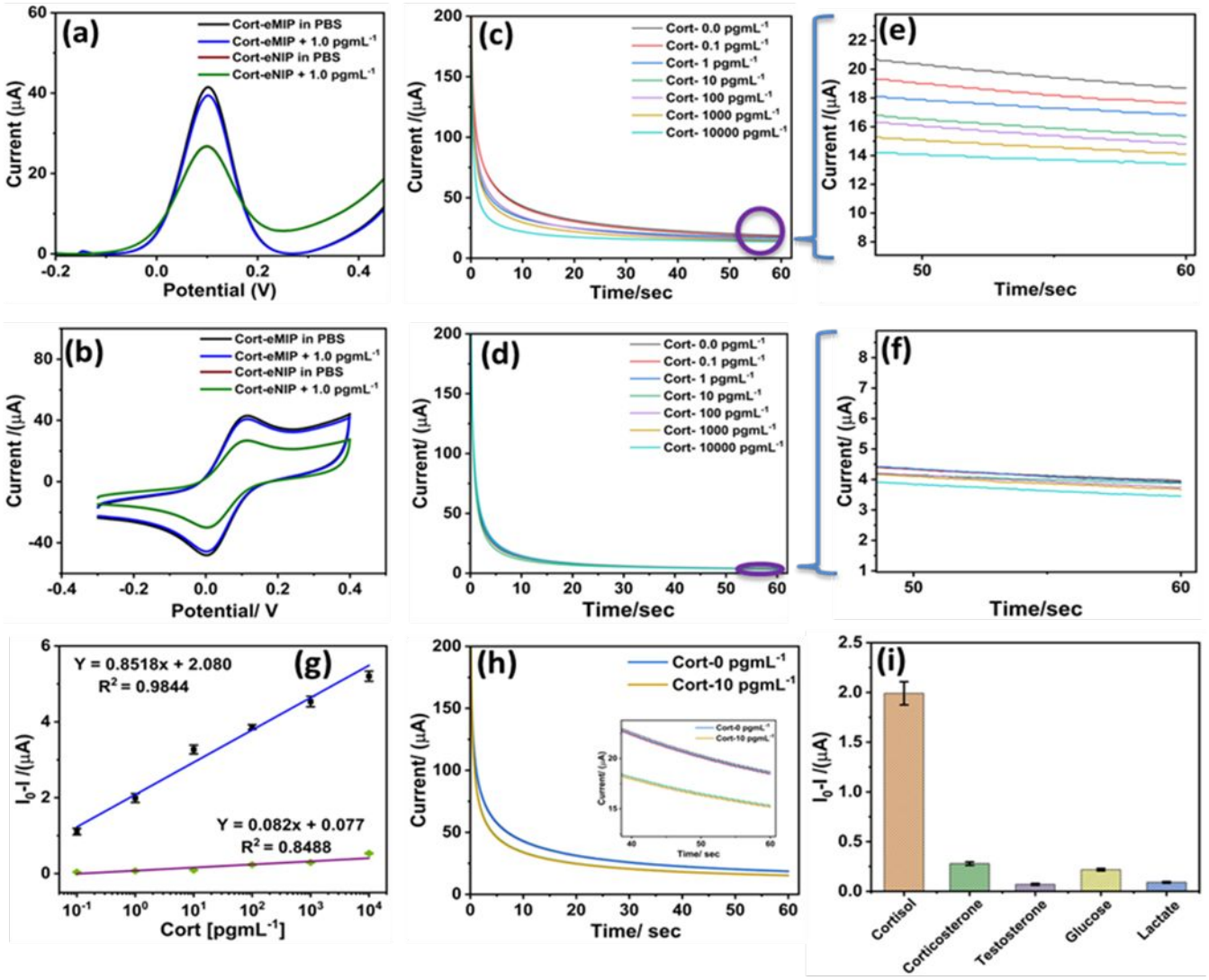

Figure 6: Characterization of cort-eMIP and cort-eNIP sensor performance. (a) differential pulse voltammogram (DPV) with and without 1.0 pg mL^{-1} cort concentration with an oxidation peak at around 0.10 V; (b) change (decrease) in current response in cyclic voltammogram (CV) with and without 1.0 pg mL^{-1} cort concentration with an oxidation peak at around 0.10 V at 0.10 V/s scan rate; (c) Chronoamperogram (CA) of the cort-eMIP sensor with increasing cortisol concentration (0.10 to 10000 pg mL^{-1}) reducing the oxidation current magnitude at 0.10 V bias; (d)) Chronoamperogram (CA) of cort-eNIP sensor with increasing cortisol concentration (0.10 to 10000 pg mL^{-1}) reducing the oxidation current magnitude at 0.10 V bias; (e and f) magnifying CA curve of eMIP and eNIP sensor for varying cort concentrations; (g) Calibration curve of cort-eMIP (blue linear-fit) and cort-eNIP (violet linear-fit) sensor in PBS (0.10 M, pH 7.4) with cortisol ranges from 0.10 to 10000 pg mL^{-1}. (h) Reproducibility performance of the sensor; (i) interference studies with structural and non-structural analogs. Each plot with an error bar depicting the replicate measurements of n = 4 sensors.

conclusively verified that the NIP film lacks selectivity for cortisol over the cort-eMIP sensor.

During the fabrication of e-NIP sensors, the absence of cortisol molecules should not lead to the formation of complementary cavities for selective cortisol binding, akin to those found in e-MIP sensors. To substantiate this assumption, we generated a calibration plot using e-NIP sensors (Fig. 6g) and cortisol solutions in spiked artificial saliva (Fig. 7a). The resulting plot, depicted in Fig. 6g, demonstrates a sensitivity of 0.082 μA log^{-1} (pg mL^{-1}) with R^2 = 0.8488 in PBS. This shows the significantly lower performance of the cort-eNIP to be deployed as a cort-sensor. Furthermore, the fabricated sensing device is meant for cortisol sensing in human saliva samples, so an additional calibration curve was constructed in cortisol-spiked artificial saliva samples. Fig. 7a demonstrates the ability of the developed sensor to quantify cortisol in spiked artificial saliva samples mimicking the real environment. Cort-eMIP sensor showed a sensitivity of 0.1655 μA log^{-1} (pg mL^{-1}), LOD of 0.08 pg mL^{-1} with R^2 = 0.9983 (n=4). In comparison, the cort-eNIP sensor showed a sensitivity of 0.012 μA log^{-1} (pg mL^{-1}), with R^2 = 0.8492 (n=4). This is one of the lowest LODs achieved using LEG-based electrodes for cortisol quantification in human saliva compared to other reports, as summarized (see supplementary table ST3).

Cortisol quantification in human saliva and validation

After performing studies in spiked artificial saliva samples, the performance of the cort-eMIP sensor was validated to quantify cortisol in human saliva samples. The procedure used for testing the saliva sample is depicted in Fig. 7b. Fig. 7b illustrates the results obtained for quantifying cortisol from a saliva sample collected from a human volunteer at Tufts University as part of a stress study (see experimental section). It is important to note that this cort-eMIP-based sensor was designed as a single-use disposable strip-based sensor that employs dielectric ink to define a sensing region, restricting the sample to this area for electrochemical measurements. The operational principle of the cort-eMIP-based sensor ensures that once cortisol molecules (the target analyte) are bound to the complementary cort-binding sites on the cort-eMIP layer, they will remain in place during subsequent measurements while measuring the signal. Consequently, each sensor strip was designed for single-use measurement purposes. In the future, if there arises a need to reuse the sensor patch, regeneration may be possible through methods such as overoxidation or incubating the sensor strip into a porogenic solvent such as methanol: acetic acid mixture [46,73].

The sensors were tested rigorously in saliva samples obtained from human subjects as part of a longitudinal stress study. The cortisol circadian rhythm refers to the 24-hour biological cycle with fluctuating cortisol levels in response to stress. Saliva samples were collected from human volunteers at various time points, including baseline, before stress induction, after stress exposure, and 20 minutes post-stress, to investigate the change in cortisol level and stress response pattern (as per approved IRB protocol for stress study mentioned in our earlier study [3]). These time points mentioned- are widely used and generally appropriate for capturing cortisol variability in response to stress [3,74]. These intervals align with the dynamics of cortisol secretion, as cortisol levels typically rise within 15–20 minutes following a stressor and then gradually return to baseline levels. Cortisol quantification was conducted on triplicate saliva samples collected from 12 human volunteers. The current signal was measured at 60-second intervals for each sample, akin to the calibration curve. Concurrently, the same samples were analysed using a commercial cortisol-ELISA kit and a Salimetric analysis for

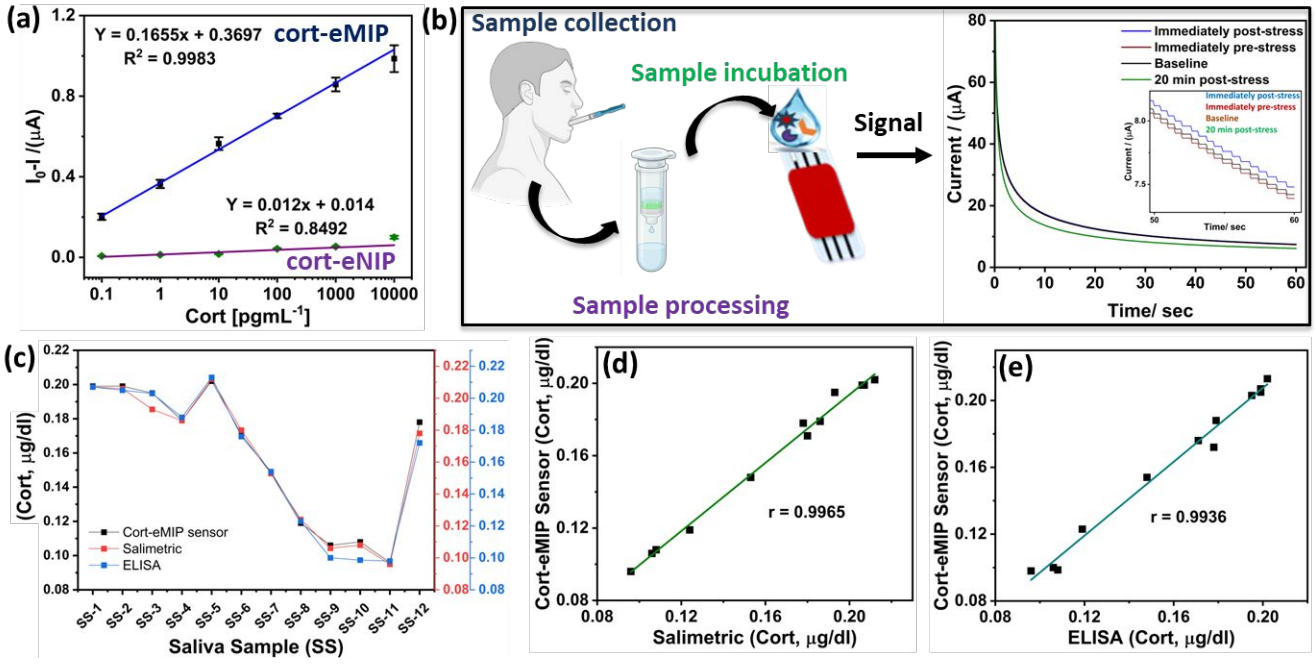

Figure 7: (a) Calibration curve in spiked artificial saliva sample with increasing cortisol ranges from 0.10 to 10000 pg mL^{-1} for cort-eMIP (blue curve) and cort-eNIP (violet curve) sensor strip; (b) Illustration of sample collection and testing for study stress level through salivary cortisol quantification (Note: Biorender was used to partly draw the Figure 7b); (c) Comparison and validation of developed cort-eMIP strip sensor with ELISA and Salimetric analysis for the same human saliva samples (*Salimetric is the third-party commercial service provider for independent measurement); establishment of correlation between cort-eMIP/LEG sensor with (d) Salimetric and (e) with ELISA methods for cortisol determination in same salivary sample.

This journal is © The Royal Society of Chemistry 20xx

salivary cortisol measurement (Fig. 7c). We calculated the regression between the cort-eMIP sensor and the cortisol ELISA kit. The results summarized in the supplementary table (ST4) show excellent agreement with less than an 8.0% standard deviation (ranging from 94.0% to 108.0%) for each testing method. These findings demonstrate that the developed cort-eMIP sensor strip is highly reliable and exhibits strong to excellent consistency and agreement with the widely used ELISA method for detecting salivary cortisol in student volunteers exposed to varying stress levels. There is a high correlation between the results obtained from the developed cort-eMIP/LEG sensor strip with Salimetric (Fig. 7d) and ELISA (Fig. 7e) with a correlation factor of r = 0.9965 (with Salimetric) and r = 0.9936 (with cortisol ELISA), respectively. The obtained comparative results validate the accuracy of rapid cortisol detection using our proposed cort-eMIP/LEG sensor. The sensor's precision, with an average coefficient of variation of less than 10 %, is comparable to that of conventional commercial methods and covers the acceptable range for cortisol detection in stress monitoring.

Conclusions

We developed an ultrasensitive and disposable biosensor strip for detecting cortisol, a potent stress biomarker, using an eMIP on a LEG electrode (known here as cort-eMIP/LEG). The sensor demonstrated a dynamic determination of 0.10 to 10000 pg mL^{-1} and a low detection limit of 20 fg mL^{-1} in saliva (S/N=3), which exceeds the requirements for cortisol levels in saliva. Requiring minimal to no sample preparation, it is highly suitable for monitoring stress in the general population anywhere. The sensor was validated on saliva samples from human volunteers who were subjected to stress. The obtained results also indicate that the cortisol sensor exhibits high reliability and strongly correlates to the on-site ELISA Standard assay. This validation was further confirmed by an external third-party service for all samples. This rigor demonstrates reliability from low sensor-to-sensor variation and scalable fabrication. While a given design with a known geometry was tested, there is considerable flexibility in choosing both the design and dimensions of the LEG electrodes owing to the nature of the direct-write capability of the laser. The scalability of the fabrication process for producing LEG electrodes and the cost-effectiveness of the raw materials used in developing the highly sensitive sensor platform are noteworthy advantages of this sensor platform.

Other salient features of the proposed eMIP/LEG-based cortisol sensors are its higher sensitivity due to increased electrode surface of LEG electrode, improved selectivity due to the use of eMIP, and the ease of reproducibility of the sensor, making this an ideal platform for point-of-care diagnostics and health monitoring. It is important to note that incorporating budget-friendly LEG-based eMIP integrated sensor strips makes it possible to deploy in a public health setting, even in resource-limited settings. Future research could enhance selectivity and reduce cross-reactivity by leveraging molecular dynamics simulations to optimize eMIP and allow one to fine-tune the materials and the polymerization process. Moreover, this eMIP/LEG sensor strip can also be developed to monitor other biomarkers, such as hormones and metabolites, whether in saliva, serum, or any other biological fluids.

Author Contributions

Atul Sharma: Conceptualization, Methodology, Experimentation, Investigation, Data curation, Validation, Formal analysis, Writing-original draft preparation and editing. **Rachel E. Owyeung**: Methodology, Investigation. **Ayanna Thomas:** Resources (Human volunteer recruitment), Writing-Reviewing, and Editing. **Sohel Siraj, Bishal Kumar Keshari, and Parikshit Sahatiya:** Data curation, Investigation. **Sameer Sonkusale:** Resources, Supervision, Project Administration, Funding Acquisition, Writing-Reviewing, and Editing. All authors have given their approval for the final version of the manuscript.

Institutional Review Board Statement:

The human saliva samples used in this study were collected during a stress study at Tufts University. The saliva sample collection procedure and protocol were approved, and samples were collected per the protocol approved by the Institutional Review Board (IRB) at Tufts University (1706030).

Conflicts of interest

The authors declare no conflicts of interest.

Data availability statements

The data supporting this article have been included as part of the Supplementary Information.

Ethical and Institutional Review Board Statement:

The human saliva samples used in this study were collected as a part of a stress study (for Social and Behavioral Sciences) conducted under a protocol approved by the Tufts Institutional Review Board (IRB) at Tufts University (Protocol#1706030). Informed consents were obtained from student volunteers participated in this study.

Acknowledgments

The authors would like to acknowledge Alia Wulff (graduate student) for saliva sample collection and Hossain Nafize Ishtiaque (graduate student) for helping with electrode fabrication. Human samples were collected following a protocol approved by the Institutional Review Board (IRB) at Tufts University (Protocol ID: 1706030). This research received support from the National Science Foundation (NSF) under Grant 1931978. It received partial funding through the TTW program at the Uniformed Services University of Health Sciences (USUHS) under award HU0001-20-2-0014 and the DoD Peer Review Medical Research Program under award number W81XWH-21-2-0012. The authors express their gratitude to the reviewers for their insightful suggestions, which have helped significantly enhance the quality of the manuscript.

References

1 K. Dhama, S. K. Latheef, M. Dadar, H. A. Samad, A. Munjal, R. Khandia, K. Karthik, R. Tiwari, M. I. Yatoo, P. Bhatt, S. Chakraborty, K. P. Singh, H. M. N. Iqbal, W. Chaicumpa and S. K. Joshi, *Front Mol Biosci*, 2019, **6**, 91.

2 G. Russell and S. Lightman, *Nat Rev Endocrinol*, 2019, **15**, 525–534.

3 A. Sharma, A. Wulff, A. Thomas and S. Sonkusale, *Microchim Acta*, 2024, **191**, 1–12.

4 R. Bruffaerts, G. Vilagut, K. Demyttenaere, J. Alonso, A. AlHamzawi, L. H. Andrade, C. Benjet, E. Bromet, B. Bunting, G. De Girolamo, S. Florescu, O. Gureje, J. M. Haro, Y. He, H. Hinkov, C. Hu, E. G. Karam, J. P. Lepine, D. Levinson, H. Matschinger, Y. Nakane, J. Ormel, J. Posada-Villa, K. M. Scott, M. Varghese, D. R. Williams, M. Xavier and R. C. Kessler, *Br J Psychiatry*, 2012, **200**, 454–461.

5 N. Dhull, G. Kaur, V. Gupta and M. Tomar, *Sens Actuators B Chem*, 2019, **293**, 281–288.

6 T. Pfaffe, J. Cooper-White, P. Beyerlein, K. Kostner and C. Punyadeera, *Clin Chem*, 2011, **57**, 675–687.

7 W. Tang, L. Yin, J. R. Sempionatto, J.-M. Moon, H. Teymourian, J. Wang, W. Tang, L. Yin, J. R. Sempionatto, J. Moon, H. Teymourian and J. Wang, *Advanced Materials*, 2021, **33**, 2008465.

8 D. S. Goldstein and B. Mcewen, *Stress*, 2002, **5**, 55–58.

9 P. Pearlmutter, G. DeRose, C. Samson, N. Linehan, Y. Cen, L. Begdache, D. Won and A. Koh, *Sci Rep*, 2020, **10**, 1–11.

10 K. Løvås and E. S. Husebye, *Eur J Endocrinol*, 2007, **157**, 109–112.

11 D. Corbalán-Tutau, J. A. Madrid, F. Nicolás and M. Garaulet, *Physiol Behav*, 2014, **123**, 231–235.

12 H. D. Ertuğrul Uygun, Z. O. Uygun, E. Canbay, F. Gïrgïn Sağın and E. Sezer, *Talanta*, 2020, **206**, 120225.

13 J. Liu, N. Xu, H. Men, S. Li, Y. Lu, S. S. Low, X. Li, L. Zhu, C. Cheng, G. Xu and Q. Liu, *Sensors*, 2020, **20**, 1422.

14 S. Kämäräinen, M. Mäki, T. Tolonen, G. Palleschi, V. Virtanen, L. Micheli and A. M. Sesay, *Talanta*, 2018, **188**, 50–57.

15 M. Yamaguchi, Y. Matsuda, S. Sasaki, M. Sasaki, Y. Kadoma, Y. Imai, D. Niwa and V. Shetty, *Biosens Bioelectron*, 2013, **41**, 186–191.

16 G. E. Abraham, J. E. Buster and R. C. Teller, *Anal Lett*, 1972, **5**, 757–765.

17 Y. H. Kim, K. Lee, H. Jung, H. K. Kang, J. Jo, I. K. Park and H. H. Lee, *Biosens Bioelectron*, 2017, **98**, 473–477.

18 A. Vasudev, A. Kaushik, Y. Tomizawa, N. Norena and S. Bhansali, *Sens Actuators B Chem*, 2013, **182**, 139–146.

19 S. K. Arya, A. Dey and S. Bhansali, *Biosens Bioelectron*, 2011, **28**, 166–173.

20 C. Tlili, N. V. Myung, V. Shetty and A. Mulchandani, *Biosens Bioelectron*, 2011, **26**, 4382–4386.

21 S. K. Arya, G. Chornokur, M. Venugopal and S. Bhansali, *Biosens Bioelectron*, 2010, **25**, 2296–2301.

22 M. Zea, F. G. Bellagambi, H. Ben Halima, N. Zine, N. Jaffrezic-Renault, R. Villa, G. Gabriel and A. Errachid, *TrAC*, 2020, **132**, 116058.

23 E. B. Bahadir and M. K. Sezgintürk, *TrAC*, 2016, **76**, 1–14.

24 M. Wang, Y. Yang and W. Gao, *Trends Chem*, 2021, **3**, 969–981.

This journal is © The Royal Society of Chemistry 20xx

Please do not adjust margins

25 S. K. Ameri, P. K. Singh and S. R. Sonkusale, *Anal Chim Acta*, 2016, **934**, 212–217.

26 S. K. Ameri, P. K. Singh and S. Sonkusale, *Biosens Bioelectron*, 2014, **61**, 625–630.

27 Y. Bai, T. Xu and X. Zhang, *Micromachines (Basel)*, 2020, **11**, 60.

28 F. Tehrani and B. Bavarian, *Sci Rep*, 2016, **6**, 1–10.

29 M. F. El-Kady, V. Strong, S. Dubin and R. B. Kaner, *Science (1979)*, 2012, **335**, 1326–1330.

30 M. F. El-Kady and R. B. Kaner, *Nat Commun*, 2013, **4**, 1–9.

31 M. G. Stanford, K. Yang, Y. Chyan, C. Kittrell and J. M. Tour, *ACS Nano*, 2019, **13**, 3474–3482.

32 J. Lin, Z. Peng, Y. Liu, F. Ruiz-Zepeda, R. Ye, E. L. G. Samuel, M. J. Yacaman, B. I. Yakobson and J. M. Tour, *Nat Commun*, 2014, **5**, 1–8.

33 R. Ye, D. K. James and J. M. Tour, *Acc Chem Res*, 2018, **51**, 1609–1620.

34 M. Coroş, S. Pruneanu and R.-I. Stefan-van Staden, *J Electrochem Soc*, 2020, **167**, 037528.

35 D. A. C. Brownson, C. W. Foster and C. E. Banks, *Analyst*, 2012, **137**, 1815–1823.

36 T. Pandhi, C. Cornwell, K. Fujimoto, P. Barnes, J. Cox, H. Xiong, P. H. Davis, H. Subbaraman, J. E. Koehne and D. Estrada, *RSC Adv*, 2020, **10**, 38205–38219.

37 M. Ren, J. Zhang and J. M. Tour, *ACS Appl Energy Mater*, 2019, **2**, 1460–1468.

38 Y. Yang, X. Fan, G. Casillas, Z. Peng, G. Ruan, G. Wang, M. J. Yacaman and J. M. Tour, *ACS Nano*, 2014, **8**, 3939–3946.

39 S. Hong, J. Kim, S. Jung, J. Lee and B. S. Shin, *ACS Mater Lett*, 2023, **5**, 1261–1270.

40 N. Baig, A. Waheed, M. Sajid, I. Khan, A. N. Kawde and M. Sohail, *Trends in Environmental Analytical Chemistry*, 2021, **30**, e00120.

41 W. Wei and X. Wang, *Materials*, 2021, **14**, 6170.

42 N. K. Singh, S. Chung, A. Y. Chang, J. Wang and D. A. Hall, *Biosens Bioelectron*, 2023, **227**, 115097.

43 J. Ok, S. Park, Y. H. Jung and T. Kim, *Advanced Materials*, 2023, **36**, 2211595.

44 S. Yeasmin, B. Wu, Y. Liu, A. Ullah and L. J. Cheng, *Biosens Bioelectron*, 2022, **206**, 114142.

45 H. Liu, W. Qin, X. Li, L. Feng, C. Gu, J. Chen, Z. Tian, J. Chen, M. Yang, H. Qiao, X. Guo, Y. Zhang, B. Zhao and S. Yin, *Anal Chem*, 2023, **95**, 16079–16088.

46 M. Kim, D. Park, J. Park and J. Park, *Biomimetics*, 2023, **8**, 282.

47 L. Özcan and Y. Şahin, *Sens Actuators B Chem*, 2007, **127**, 362–369.

48 S. Sadki, P. Schottland, N. Brodie and G. Sabouraud, *Chem Soc Rev*, 2000, **29**, 283–293.

49 A. N. Hasanah, N. Safitri, A. Zulfa, N. Neli and D. Rahayu, *Molecules 2021*, 2021, **26**, 5612.

50 K. Fremielle Lim and C. I. Holdsworth, *Molecules*, 2018, **23**, 2996.

51 P. Manickam, R. E. Fernandez, Y. Umasankar, M. Gurusamy, F. Arizaleta, G. Urizar and S. Bhansali, *Sens Actuators B Chem*, 2018, **274**, 47–53.

52 S. P. Özkorucuklu, Y. Şahin and G. Alsancak, *Sensors*, 2008, **8**, 8463–8478.

53 V. Ratautaite, U. Samukaite-Bubniene, D. Plausinaitis, R. Boguzaite, D. Balciunas, A. Ramanaviciene, G. Neunert and A. Ramanavicius, *Int J Mol Sci*, DOI:10.3390/IJMS22095032.

This journal is © The Royal Society of Chemistry 20xx

54 C. Malitesta, E. Mazzotta, R. A. Picca, A. Poma, I. Chianella and S. A. Piletsky, *Anal Bioanal Chem*, 2012, **402**, 1827–1846.

55 R. A. Lorenzo, A. M. Carro, C. Alvarez-Lorenzo and A. Concheiro, *Int J Mol Sci*, 2011, **12**, 4327–4347.

56 A. C. Ferrari, *Solid State Commun*, 2007, **143**, 47–57.

57 A. Lamberti, F. Clerici, M. Fontana, L. A. Scaltrito Lamberti, F. Clerici, M. Fontana and L. Scaltrito, *Adv Energy Mater*, 2016, **6**, 1600050.

58 J. E. L. Villa, S. Khan, L. C. S. Neres and M. D. P. T. Sotomayor, *Journal of Polymer Research*, 2021, **28**, 1–9.

59 S. xuan Zhou, X. tong Lin, J. Wang, H. xiang Wang and G. tang Chen, *Food Chem*, 2023, **421**, 136196.

60 A. George, A. R. Cherian, L. Benny, A. Varghese and G. Hegde, *Microchemical Journal*, 2023, **184**, 108155.

61 E. Mazzotta, S. Rella, A. Turco and C. Malitesta, *RSC Adv*, 2015, **5**, 83164–83186.

62 A. R. Cherian, L. Benny, A. George, U. Sirimahachai, A. Varghese and G. Hegde, *Electrochim Acta*, 2022, **408**, 139963.

63 S. Han, C. Liu, N. Li, S. Zhang, Y. Song, L. Chen, M. Xi, X. Yu, W. Wang, M. Kong and Z. Wang, *CrystEngComm*, 2022, **24**, 1866–1876.

64 Z. Wan, M. Umer, M. Lobino, D. Thiel, N. T. Nguyen, A. Trinchi, M. J. A. Shiddiky, Y. Gao and Q. Li, *Carbon N Y*, 2020, **163**, 385–394.

65 N. H. Barbhuiya, A. M. Nair, N. Dixit and S. P. Singh, *ACS Omega*, 2024, **9**, 22819–22830.

66 P. Zhao, Y. Zhang, Y. Liu, D. Huo, J. Hou and C. Hou, *Biosens Bioelectron*, DOI:10.1016/J.BIOS.2024.116012.

67 B. Gupta, N. Kumar, K. Panda, V. Kanan, S. Joshi and I. Visoly-Fisher, *Scientific Reports 2017 7:1*, 2017, **7**, 1–14.

68 W. Song, J. Zhu, B. Gan, S. Zhao, H. Wang, C. Li and J. Wang, *Small*, 2018, **14**, 1702249.

69 N. H. Barbhuiya, A. M. Nair, N. Dixit and S. P. Singh, *ACS Omega*, 2024, **9**, 22819–22830.

70 A. Sorribes-Soriano, F. A. Esteve-Turrillas, S. Armenta, P. Amorós and J. M. Herrero-Martínez, *Anal Chim Acta*, 2019, **1052**, 73–83.

71 M. A. Isaacs, J. Davies-Jones, P. R. Davies, S. Guan, R. Lee, D. J. Morgan and R. Palgrave, *Mater Chem Front*, 2021, **5**, 7931–7963.

72 K. Ngamchuea, S. Eloul, K. Tschulik and R. G. Compton, *Journal of Solid State Electrochemistry*, 2014, **18**, 3251–3257.

73 N. A. Shama, S. Aşır, I. Göktürk, F. Yılmaz, D. Türkmen and A. Denizli, *ACS Omega*, 2023, **8**, 29202–29212.

74 Y. Maruyama, A. Kawano, S. Okamoto, T. Ando, Y. Ishitobi, Y. Tanaka, A. Inoue, J. Imanaga, M. Kanehisa, H. Higuma, T. Ninomiya, J. Tsuru, H. Hanada and J. Akiyoshi, *PLoS One*, 2012, **7**, e39375.

This journal is © The Royal Society of Chemistry 20xx

Data availability statements

The data supporting this article have been included as part of the Supplementary Information.